Int. J. Plant Sci. 174(3):499–510. 2013.

1058-5893/2013/17403-0019$15.00 DOI: 10.1086/668694

AERODYNAMIC CHARACTERISTICS OF SACCATE POLLEN GRAINS

Lisa Grega,[1,]* Sean Anderson,* Matthew Cheetham,* Matthew Clemente,* Alex Colletti,* Winston Moy,* David Talarico,* Scott L. Thatcher,† and Jeffrey M. Osborn‡

*Department of Mechanical Engineering, College of New Jersey, Ewing, New Jersey 08628, U.S.A.; †Department of Mathematics and Computer Science, Truman State University, Kirksville, Missouri 63501, U.S.A.; and ‡Department of Biology, College of New Jersey, Ewing, New Jersey 08628, U.S.A.

The pollen grains of several gymnosperm groups consist of a main body and one to three air-filled bladders, or sacci. Although sacci may serve a buoyancy function to orient the grain on the ovular pollination droplet in some taxa, sacci have also been shown to increase pollen volume while adding minimal mass, thus decreasing density and thereby increasing the aerodynamic efficiency of wind pollination. However, no published studies have quantitatively addressed the effects of grain geometry or surface ornamentation at the low Reynolds numbers that pollen grains demonstrate. The objectives of this study were to empirically investigate the effects of varying geometries and surface ornamentation on the aerodynamic properties of saccate pollen grains through the experimental determination of drag coefficients and shape factors. Structurally different grains of two extant conifers (*Pinus* and *Falcatifolium*) were studied, and using electron microscopy, mathematical modeling, and solid modeling, we created scaled-up physical models of the pollen types. Models were produced with and without sacci, as well as with and without surface texture on the main body. Sacci increased the shape factor, or resistance coefficient, in all pollen types studied, compared to the same types that had been modeled without sacci. The presence of surface ornamentation also decreased the drag coefficients for saccate pollen grains of *Pinus*. This study is the first to experimentally demonstrate the effect of surface texture on drag for any biological or nonbiological particle at low Reynolds numbers. This study also provides additional empirical evidence for the aerodynamic role of sacci, supporting their adaptive significance for anemophily.

Keywords: anemophily, Coniferales, exine ornamentation, *Falcatifolium*, *Pinus*, pollen geometry, saccate pollen, wind pollination.

Introduction

Wind pollination has historically been thought to be a random and wasteful process, in which significant amounts of pollen are produced, with relatively few individual pollen grains reaching the ovulate structures. However, several studies have shown that anemophily is facilitated and enhanced by reproductive characters with efficient aerodynamic properties (Whitehead 1983; Niklas 1984, 1985*a*, 1985*b*). For example, with regard to ovulate cones, cone positions on branches, needle positions around cones, and the harmonic motion of branches caused by wind, all contribute to aerodynamic efficiency. Recirculation regions around cones also create pockets into which pollen grains are entrained and remain for extended periods of time, thereby increasing the probability of entrapment by the ovule (Niklas and Paw U 1982).

The morphology of some pollen grain types also has been hypothesized to increase the aerodynamic efficiency of wind pollination, resulting in increased dispersal distances. In particular, pollen grains of several gymnosperm groups consist of a main body and one to three air-filled bladders, or sacci (Osborn and Taylor 1994; Taylor et al. 2009). The main body houses the microgametophytic cells and is protected by a structurally complex pollen wall. The outer layer of the pollen wall expands outward from the main body to form the sacci. Although several studies have conjectured and shown that sacci serve a buoyancy function to properly orient the grain on the pollination droplet within the ovule (Tomlinson 1994, 2000; Runions et al. 1999; Leslie 2010), sacci have also been hypothesized to significantly increase the volume of the pollen grain while adding minimal mass, thus decreasing its density (Wodehouse 1935; Proctor et al. 1996). This would result in greater flow resistance and lower settling velocity, allowing for greater dispersal distances in wind.

Until recently, no published studies had empirically tested the aerodynamic hypothesis for the role of sacci. Schwendemann et al. (2007) studied structurally different extant and extinct pollen types and developed a mathematical model that, for the first time, quantitatively demonstrated that sacci reduced the settling velocities of saccate pollen types, thus increasing dispersal distances. Only when the sacci added significant mass (and hence overall pollen density) as a result of thick pollen walls and/or dense endoreticulations, as in the extant conifer *Falcatifolium* and the fossil seed fern *Caytonanthus*, did the settling velocity increase (Schwendemann et al. 2007).

The mathematical model developed by Schwendemann et al. (2007) was the first to apply structural characteristics of pollen grains as directly measured using scanning electron

[1] Author for correspondence; e-mail: grega@tcnj.edu.

Manuscript received April 2012; revised manuscript received October 2012.

microscopy (SEM) and transmission electron microscopy (TEM) to compute settling velocities analytically. When these structural characters were used, the grain's mass and volume were accurately determined, from which the settling velocity was calculated. The mathematical model required as a final input variable the drag coefficient, which was estimated by assuming the pollen shapes to be spheroids. The advantage of such a model is that the sacci could be "removed," allowing for direct examination of the effect of the sacci on settling velocity. Furthermore, settling velocities of extinct taxa could be determined, on the basis of well-preserved structural characters obtained from fossil pollen grains.

The drag coefficients used in the mathematical model of Schwendemann et al. (2007) to calculate settling velocities were estimated on the basis of existing data for two generalized spheroid geometries, oblate and prolate spheroids (Vogel 1994). However, saccate pollen grains have unique geometrical attributes that are not accurately represented by these generalized spheroids. For example, grain geometry can be influenced by several factors; the physical orientation of the sacci varies as a function of hydration state, there is considerable variability in saccus size, and grains exhibit a high degree of variation in fore-aft asymmetry with respect to their direction of travel. Moreover, the pollen grains studied by Schwendemann et al. (2007) were not smooth; however, at the time, surface ornamentation was not incorporated into the mathematical model. In fact, no published studies have quantitatively addressed the effects of surface roughness on particles, biological or nonbiological, at the low Reynolds numbers that pollen grains demonstrate.

A Reynolds number is an important aerodynamic attribute that represents the ratio of inertial effects (i.e., the product of the particle's velocity and length scale) to viscous effects (i.e., viscosity of the medium/fluid in which the particle is moving—in this case, air). Biological particles typically exhibit very low Reynolds numbers because of their small size and speed of travel. The pattern of fluid flow around particles that have very low Reynolds numbers is typically characterized by minimal separation of the flow, as well as smooth, well-defined flow paths.

The objectives of this study were to empirically investigate the effects of varying geometries and surface ornamentation on the aerodynamic properties of saccate pollen grains through the experimental determination of drag coefficients and shape factors. Structurally different grain types were selected because wind dispersal of saccate pollen grains is influenced by many factors, including variability in pollen geometry while airborne and unique surface textures.

Material and Methods

Physical Scale Models

Two conifer species with saccate pollen were selected for this study: *Pinus strobus* L. (Pinaceae) and *Falcatifolium taxoides* (Brongn. & Gris) de Laub. (Podocarpaceae). These taxa and two pollen grain types of each were chosen for the study on the basis of the geometrical diversities of the pollen grains, as well as the distinctly different effects of their sacci on settling velocity as found in Schwendemann et al. (2007). The four grains were chosen because they exhibited considerable differences among overall grain geometry, sacci size, and sacci position (e.g., angle of rotation) relative to the main body. The grains are referred to here by their experimental/accession numbers (*Pinus* 13, *Pinus* 25, *Falcatifolium* 69, and *Falcatifolium* 83); SEM micrographs of the four grains are shown in figure 1*a*–1*d*.

Mathematical renderings of the grains were formulated using the software Mathematica (fig. 1*e*–1*h*); these were based on generalized equations for ellipsoids and the structural measurements made by Schwendemann et al. (2007). The Mathematica models were then imported into the solid-modeling software Pro/Engineer (Pro/E) in order to produce scaled three-dimensional renderings (fig. 1*i*–1*l*) from which physical models could be created. Each Pro/E model in the software was scaled up by a factor of 400–600 to produce a maximum length scale of ~25 mm. To determine the effects of sacci, Pro/E models were produced for each pollen grain type that (*a*) contained sacci in authentic orientations and sizes and (*b*) had the sacci removed, representing only the main body.

Using the SEM micrographs depicting the surface ornamentation innate to each pollen type, we incorporated similar patterns into the Pro/E models of the two *Pinus* pollen types (fig. 2). The texture consisted of hemispherical elements formed on the surface of the main body only; the sacci were left smooth, as in the actual pollen grains. The degree of surface texture (or "roughness") and the relative dimensions of the individual sculptural elements included on the models were rendered to scale. These calculations were determined on the basis of examination of TEM micrographs (height of the sculptural elements) and SEM micrographs (width/diameter of the sculptural elements) of the actual pollen grains to be modeled.

The Pro/E models were then printed on a ThermoJet stereolithography-based three-dimensional printer. The three-dimensional printer constructed two hollow halves of each model, which were filled with small steel spheres to produce the desired density. On the basis of the pollen grains' individual structural characteristics described in Schwendemann et al. (2007), the ratio of the masses of the entire pollen grain divided by the mass of the body was calculated. Because physical models of the main body only were also created, the mass of the main body component of the model was known. Consequently, different amounts of weight could be added to the main body and sacci until the desired mass ratio was achieved that matched the mass ratio of the actual grains, thus ensuring that the models would fall in the same manner. The steel spheres were lined around the inside of the model in order to uniformly distribute the weight. Once the desired weight was achieved, the two halves were sealed using a thin bead of epoxy; the epoxy was microns thick and did not leave a residue or contribute relevant mass. The density of each model was indirectly determined by measuring the dry mass of the model, as well as its mass submerged in distilled water. A Mettler analytic scale with a resolution of 0.0001 g was used for all weight measurements. This technique was validated by measuring the densities of smooth delrin spheres and comparing them with their densities based on sphere mass and volume. Agreement to within 0.2% was achieved.

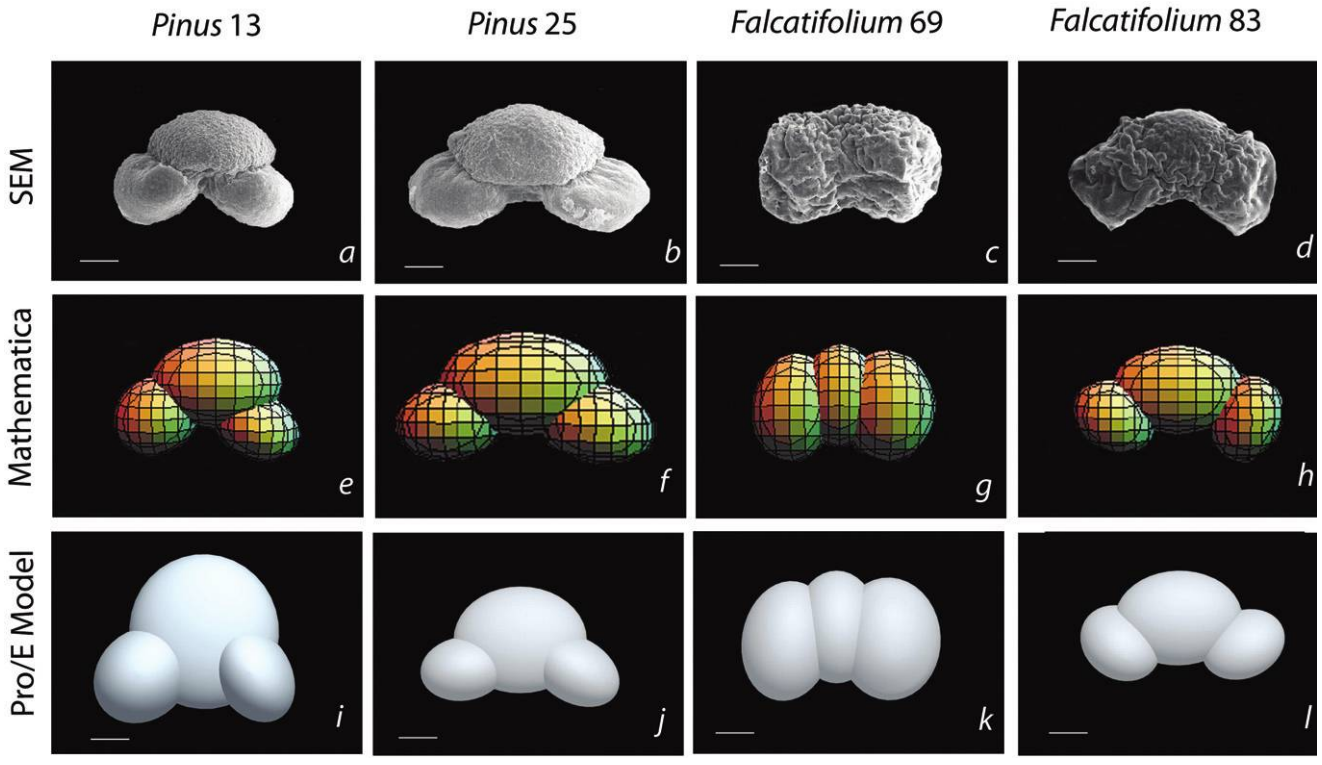

Fig. 1 Images of four pollen types studied: *Pinus* 13 (*a*, *e*, *i*), *Pinus* 25 (*b*, *f*, *j*), *Falcatifolium* 69 (*c*, *g*, *k*), and *Falcatifolium* 83 (*d*, *h*, *l*). *a–d*, Scanning electron microscope (SEM) images (scale bars = 10 μm). *e–h*, Mathematical renderings of grains formulated using Mathematica software. *i–l*, Mathematica models imported into solid-modeling software Pro/Engineer (Pro/E) to produce scaled three-dimensional renderings. Each model in software scaled up by a factor of 400–600 (scale bars = 5 mm).

Settling Velocity Experiments

Experiments were conducted in a rectangular tank of dimensions 20 cm × 20 cm and a depth of 60 cm. The front wall of the tank was constructed of clear Plexiglas to enable viewing of the physical models. The tank was filled with glycerin to within 8 cm of the top. This choice of fluid dictated the ultimate masses of the physical scale models, as their densities were designed to be just slightly greater than that of the glycerin so they would fall at low enough speeds to generate the desired Reynolds number range. The primary reason for using glycerin as the working fluid was that its kinematic viscosity varies by roughly a factor of six over a temperature range between 10° and 30°C. Thus, Reynolds numbers could be varied using a small set of physical scale models of the pollen grains.

To maintain the tank in the desired temperature range, we conducted the experiments in an environmental chamber ~2.4 m × 2.4 m × 2.4 m in dimension. Both temperature and humidity in the chamber were accurately controlled such that during a given set of runs, the glycerin temperature did not vary by more than 0.1°C in the center of the tank. Kinematic viscosity was measured using a Cannon Ubholde viscometer submerged in a cylindrical water bath.

A LaVision imaging system was used for measurement of settling velocities and flow fields around the physical scale models as they fell through the glycerin-filled tank. When the settling velocities were measured, each physical model was released from rest at the surface and filmed using a CCD video camera at a rate of 8 frames/s. As controls, both smooth and textured spheres were studied as well. Recorded images were then analyzed to determine translation distance over a given number of frames. Additionally, each model's speed at the top and bottom of the field of view was checked to ensure steady fall velocity.

A qualitative experiment was also conducted to visualize the wake flow behind some of the physical models and control spheres. The models and spheres were coated with dyed glycerin and released into the tank. This resulted in a trail of dyed fluid left behind the model as it passed through the camera's field of view. The Reynolds numbers for the *Pinus* 25 models and control spheres studied in these experiments were maintained within the appropriate value range, varying between 0.1 and 0.5.

Modeling Nonspherical Particle Drag at Low Reynolds Numbers

Despite the fact that the vast majority of biological and nonbiological particles are irregularly shaped, it is not possible to analytically calculate drag coefficients tailored to specific geometric variations. Drag coefficients are highly dependent on both shape and Reynolds number. The Reynolds number is defined as

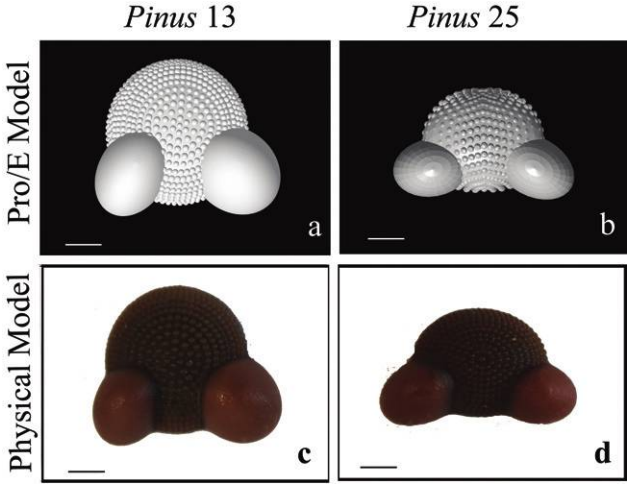

Fig. 2 Pollen models of two *Pinus* grains studied depicting surface ornamentation, *Pinus* 13 (*a*, *c*) and *Pinus* 25 (*b*, *d*). *a*, *b*, Pro/Engineer (Pro/E) models of two *Pinus* pollen types depicting surface ornamentation on main bodies and smooth sacci (scale bars = 5 mm). *c*, *d*, Pro/E models shown in *a* and *b* printed on three-dimensional printer to produce physical scale models (scale bars = 5 mm).

$$\mathrm{Re} = \frac{\rho_f V L}{\mu}, \tag{1}$$

where V is the particle velocity, L is a characteristic length (the major axis length perpendicular to the direction of flow), and ρ_f and μ represent the fluid density and dynamic viscosity, respectively. Physically, this parameter represents the ratio between inertial and viscous effects; at low Reynolds numbers, viscous effects dominate. As a result, a particle released from rest will reach its terminal velocity very quickly, so particle acceleration is negligible. This allowed for a simple force balance to be performed in which the particle's weight was balanced by its buoyancy and drag forces. A particle's drag force, F_D, was then calculated as

$$F_D = m_p g\left(1 - \frac{\rho_f}{\rho_p}\right), \tag{2}$$

where m_p and ρ_p represent the particle mass and density, respectively. The coefficient of drag, C_D, was defined as

$$C_D = \frac{F_D}{0.5\rho_f V^2 A}, \tag{3}$$

where A is the projected area of the particle normal to the flow direction.

The one geometry that has been extensively studied and for which analytical solutions can be obtained is the sphere. At low Reynolds numbers, the drag force on a sphere was derived by Stokes (1851) to be

$$F_D = 3\pi\mu V d, \tag{4}$$

in which d is the sphere diameter. The drag coefficient for a sphere then becomes

$$C_D = \frac{24\mu}{\rho V d} = \frac{24}{\mathrm{Re}}. \tag{5}$$

Analytical and numerical solutions for spheroids, which are essentially spheres elongated in one direction, have been obtained by Aoi (1955) and Breach (1960), among others. Even though the geometry is still relatively simple, the resulting expressions for the drag coefficient become considerably more complex than that given above for a sphere. However, most regularly shaped nonspherical particles, such as cylinders or cones, do not have analytical solutions.

To address the geometrical complexities introduced by irregular particle shapes, empirical approaches have been taken in order to apply Stokes's (1851) simple solution to other geometries. This involved defining an equivalent sphere diameter and a shape correction factor (McNown and Malaika 1950; Murphy et al. 2002; Loth 2008). This equivalent sphere, or nominal diameter d_n, was defined in this study, following the approach of McNown and Malaika (1950), as the diameter of a spherical particle containing the same volume as the nonspherical particle of interest. Conceptually, this would involve "repackaging" the nonspherical particle into a spherical shape. This repackaged sphere would have a diameter d_n. The shape correction factor is an empirical coefficient, which relates the drag force or drag coefficient of an irregularly shaped particle to that of a sphere. McNown and Malaika (1950) used this shape factor to extend Stokes's (1851) law (eq. [4]) to any nonspherical particle at a low Reynolds number:

$$F = (3\pi\mu V d_n)K, \tag{6}$$

where V is the settling velocity of the nonspherical particle and d_n is the nominal diameter of the particle, which can be calculated using the following definition:

$$d_n = \left(\frac{6\forall}{\pi}\right)^{1/3}. \tag{7}$$

In equation (7), $\forall$ represents the volume of the nonspherical particle. The shape factor K is also referred to as a resistance coefficient. Because the drag force on two particles of the same weight and volume will be equal, equations (4) and (6) were combined, resulting in an interpretation of K as a velocity ratio:

$$K = \frac{V_s}{V}, \tag{8}$$

in which V_s represents the velocity of a sphere with a diameter equal to the nominal diameter of the particle. A shape factor greater than 1 can then be interpreted as the velocity of the nonspherical particle being less than that of an equivalent sphere, meaning that its drag coefficient would be higher than that of a sphere. The determination of shape factors was therefore a useful means to compare the effect of a particle's geometry on its drag coefficient and, ultimately, its settling velocity.

Calculating Drag Coefficients and Shape Factors

Drag coefficients of the models were computed using equation (3). The projected area was obtained from the Pro/E

solid-modeling software. The settling velocities had to be corrected for wall effects, as the physical boundaries of the tank would result in the models dropping at a slower velocity than they would in an unbounded medium. Correction curves developed by McNown and Malaika (1950) were applied on the basis of the ratio of the model-to-tank size. Furthermore, because the correction curves were derived for a cylindrical tank and the measurements were made in a square tank, an additional correction relation derived by Happel and Bart (1974) was used to compute an equivalent tank diameter. Because the models were not spherical, the square root of the ratio of the projected area of the model to the area of the equivalent cylinder was used as a diameter ratio for all corrections.

During each set of drops at a given temperature, smooth delrin spheres were also dropped; these served as a calibration check for the results. Drag coefficients of the delrin spheres were calculated and compared with the drag coefficient correlation developed by Clift et al. (1978) for a general sphere. This correlation is given by the expression

$$C_D = \frac{24}{Re}\left[1 + 0.1315 \times Re^{(0.82-0.05\log Re)}\right]. \quad (9)$$

Agreement between the measured sphere drag coefficients and equation (9) was achieved to within 3%.

In order to calculate the shape factor (K) associated with each model, equation (2) was first applied to calculate the drag force of the model. This was then inserted into equation (6), along with the model's measured settling velocity and calculated nominal diameter (eq. [7]), in order to solve for K. These shape factors were then used to calculate settling velocities of the actual pollen grains being modeled. This was done by applying the grain's structural measurements to equations (2) and (6).

Uncertainties in the drag coefficients to be presented were calculated on the basis of uncertainties in measurements of the model density, fluid density, projected area, mass, and settling velocity. On the basis of multiple drops of each physical model, uncertainty in settling velocity was estimated to be 2%. The fluid density was measured using a hydrometer with an uncertainty of 0.5%, and the model's density carries an uncertainty of 0.2%, as discussed previously. These values produced an average overall uncertainty in drag coefficient of 5%.

Results

Pollen Geometry

The two taxa and four pollen types studied (*Pinus* 13, *Pinus* 25, *Falcatifolium* 69, and *Falcatifolium* 83) exhibited different saccus and main body sizes, as well as saccus orientation patterns (figs. 1, 3). The sacci on *Falcatifolium* 69, for example, are relatively large compared to the main body size. Regarding the angle of orientation, the sacci of this grain are splayed out to the sides of the main body more so than in comparison with the other grains (fig. 1). In contrast, *Pinus* 13 has a relatively large main body size compared to the saccus size, and its sacci are positioned closer together. On the basis of the principal axis ratios of the physical models, the saccate grains of *Falcatifolium* could be considered spheroidal, as one of the principal axis ratios is equal to 1 (fig. 3). However, this is only from the perspective of circumscribing a spheroidal area around the grain. The circumscribed *Pinus* geometries are ellipsoidal (i.e., both principal axis ratios are different from 1; fig. 3); consequently, it is important to note that each grain is geometrically unique, asymmetrical, and three dimensional in nature.

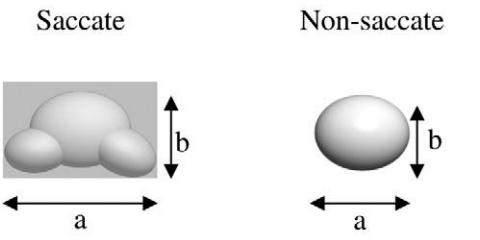

Taxon	Saccate a/b	Saccate a/c*	Non-saccate a/b	Non-saccate a/c*
Pinus 13	0.84	1.2	0.97	1.5
Pinus 25	0.59	1.2	0.80	1.2
Falcat 69	0.64	1.0	0.97	1.35
Falcat 83	0.53	1.0	0.75	1.1

Fig. 3 Principal axis ratios of pollen models with sacci and without sacci (main body only). Note that dimension c is normal to the page.

The effects of sacci. These geometrical effects were comparatively examined among the four grain types, as well as between saccate and nonsaccate pollen models of the same pollen types. To isolate the effect of sacci, models were created for each pollen grain type without surface ornamentation (i.e., smooth models), and these smooth models were created both with and without sacci. Drag coefficients were experimentally determined for each of the saccate pollen models using the measured settling velocities and equation (3), and the drag coefficients were then plotted as a function of Reynolds number (fig. 4). Figure 4 also shows the drag coefficients for each of the pollen models relative to the variation in drag coefficient for a control sphere (using the correlation given by eq. [9]). All four pollen models exhibited higher drag coefficients than that of a sphere, with *Falcatifolium* 83 having the highest drag coefficient, followed by *Pinus* 25 (fig. 4). These two models have comparably sized sacci and positioning relative to the main body; however, the angle of orientation of the sacci differs between *Falcatifolium* 83 and *Pinus* 25, with the major axis of the *Pinus* sacci being oriented into the main body (figs. 1, 3). These data indicate that geometrical attributes of the pollen grains empirically have an impact on pollen drag.

On the basis of measurements of the structural characteristics, masses for the main bodies and sacci were determined for each pollen type (table 1). When each section was represented as an ellipsoid, volumes and cross sections were also calculated specific to each grain type. Using this information,

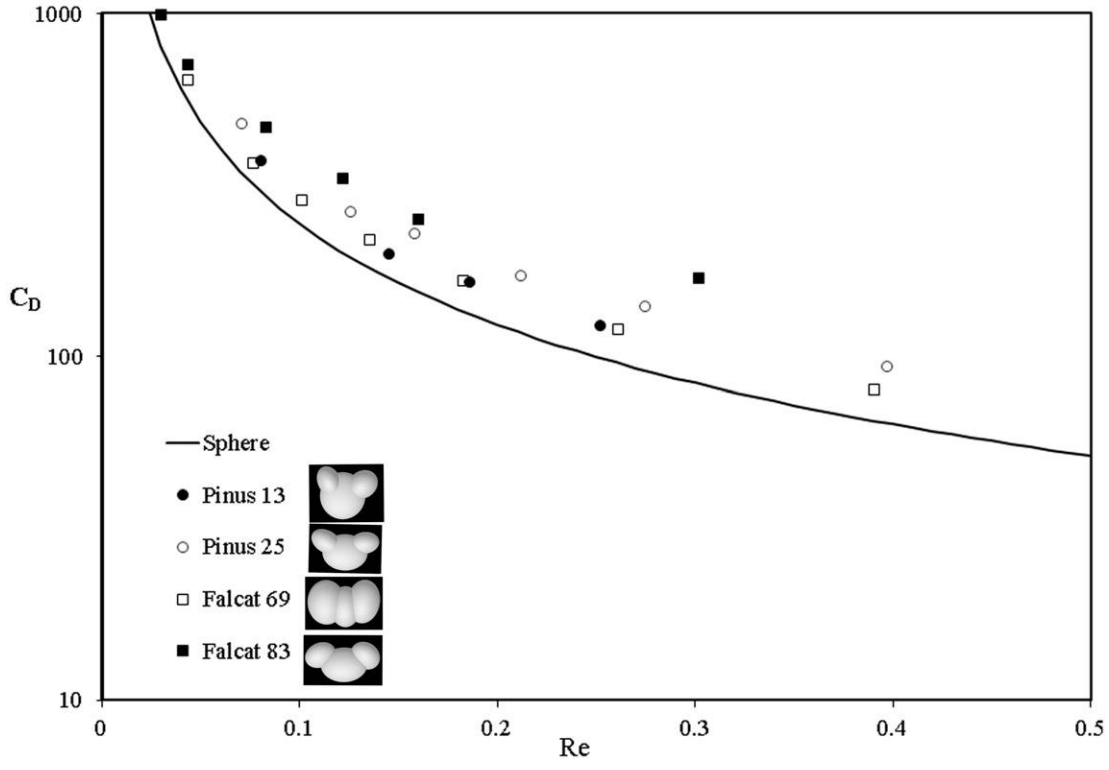

Fig. 4 Effects of pollen geometry on drag. Drag coefficient (C_D) versus Reynolds number (Re) for four pollen types. Pollen types modeled here are all smooth and did not include surface texture on main body. Control sphere represents standard curve from Clift et al. (1978). All four pollen models exhibited higher drag coefficients than that of a sphere, with *Falcatifolium* 83 having the highest drag coefficient, followed by *Pinus* 25.

we calculated the drag force of each grain using equation (2). The sacci on the two *Pinus* grains add ~70% more volume to the size of the grains while adding only ~10% more mass (table 1). In contrast, whereas the sacci on the two *Falcatifolium* grains also add considerable volume, they also add substantial mass (table 1), thus lending support to the notion that sacci of this genus increase settling velocities. These data are used below to predict settling velocities of the actual grains.

Shape factors and settling velocities. Shape factors (K) were calculated for both the saccate and nonsaccate models of each pollen type and plotted as a function of the logarithm of the Reynolds number (fig. 5). Shape factors, like drag coefficients, are a measure of a particle's resistance to flow, with larger resistance leading to lower settling velocities. At very low Reynolds numbers (Stokes range), the curves begin to level out and approach a constant value of K. At higher Reynolds numbers, above ~0.1, inertial effects cause increases in the shape factor (fig. 5). In the constant Stokes range, the nonsaccate models of all four grain types have very similar values, varying between slightly less than 1 to slightly greater

Table 1

Structural Characteristics of Pollen Grains and Associated Drag Forces

	Grain characteristics			
Taxon	Mass (m_p, g)	Volume (V, cm^3)	Density (ρ_p, g/cm^3)	Drag force (F_D, $g\ cm/s^2$)
Pinus 13:				
With sacci	1.67×10^{-8}	2.39×10^{-8}	.70	1.63×10^{-5}
Without sacci	1.48×10^{-8}	1.39×10^{-8}	1.06	1.45×10^{-5}
Pinus 25:				
With sacci	2.50×10^{-8}	3.58×10^{-8}	.70	2.45×10^{-5}
Without sacci	2.26×10^{-8}	2.14×10^{-8}	1.06	2.21×10^{-5}
Falcatifolium 69:				
With sacci	1.31×10^{-8}	1.76×10^{-8}	.74	1.28×10^{-5}
Without sacci	6.52×10^{-9}	5.71×10^{-9}	1.14	6.38×10^{-6}
Falcatifolium 83:				
With sacci	1.50×10^{-8}	1.75×10^{-8}	.86	1.47×10^{-5}
Without sacci	1.02×10^{-8}	9.04×10^{-9}	1.13	9.97×10^{-6}

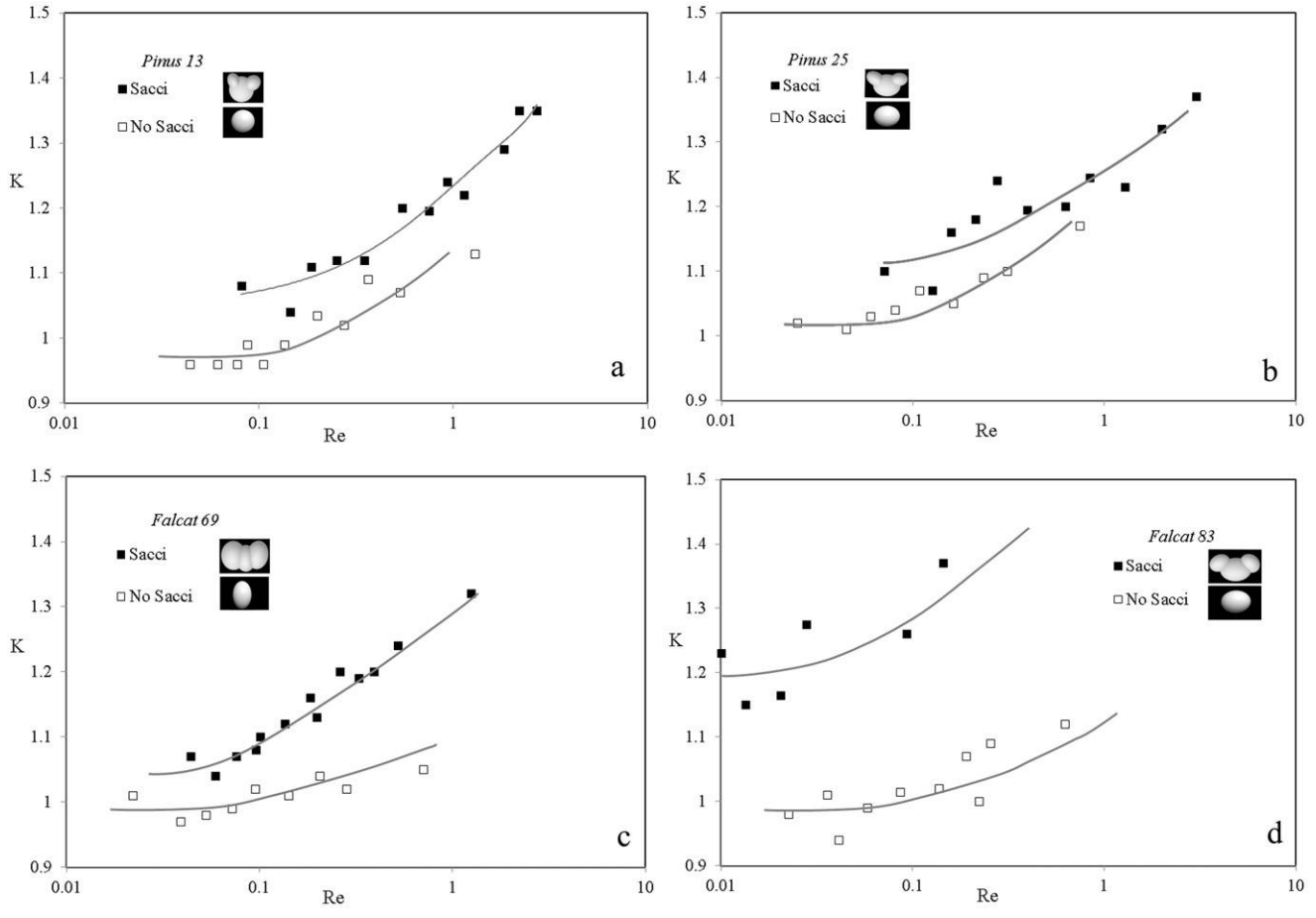

Fig. 5 Effects of pollen geometry on drag. Shape factor (K) versus Reynolds number (Re) for four pollen types. *a*, *Pinus* 13. *b*, *Pinus* 25. *c*, *Falcatifolium* 69. *d*, *Falcatifolium* 83. Each pollen type modeled both with sacci (filled squares) and without sacci (i.e., main body only; open squares). In all cases, saccate pollen grains demonstrated higher shape factors. All pollen types modeled were smooth and did not include surface texture on the main body. Nonsaccate models of all four grain types have very similar values, varying between slightly less than 1 to slightly greater than 1. Shape factors for saccate models all higher by 10%–20% than their nonsaccate counterparts, with *Falcatifolium* 83 producing the highest shape factor, followed by *Pinus* 13.

than 1 (fig. 5). The shape factors for the saccate models are all higher by 10%–20% than their nonsaccate counterparts, with *Falcatifolium* 83 producing the highest shape factor of ~1.4 (fig. 5), followed by *Pinus* 13. These data are consistent with the trends exhibited in the drag coefficient plot (fig. 4).

Using the experimentally determined shape factors, we applied equations (2) and (7) to the pollen grain structural data (table 1) in order to predict the settling speeds of the grains. These experimentally predicted settling speeds were then compared to those predicted using the mathematical model (table 2). The shape factors that were used for each model were averaged values in the Stokes regime. Using experimentally determined shape factors results in predictions of settling speeds that are in excellent agreement (within 5%) with the mathematical model's predictions (table 2). These shape factor data also confirm that sacci reduce settling speeds in the *Pinus* pollen grains, whereas sacci increase settling speeds in *Falcatifolium*.

Surface Ornamentation

To evaluate the effects of surface ornamentation on aerodynamic properties, we calculated drag coefficients from measured settling speeds of smooth and textured pollen models of *Pinus* (fig. 6). These textured models were compared with nontextured, smooth models of the same grain type. For both *Pinus* 13 and *Pinus* 25, the textured models exhibited a decrease in drag coefficient over a wide range of Reynolds numbers when compared with the nontextured, smooth models (fig. 6).

Surface ornamentation and the presence of sacci. The lower drag coefficients here would theoretically increase the pollen grains' settling speeds, as these result in a lower resistance to the flow. However, given the unique asymmetrical shapes of the pollen grains, along with the location and orientation of the sacci on the aft region of the main bodies relative to the flow direction, the presence of sacci also plays a role in the flow dynamics producing this effect. The aerodynamic impact of the sacci here was ascertained by measuring

Table 2

Comparison of Pollen Settling Speeds between Predictions Using Experimentally Determined Shape Factors and Mathematical Model's Prediction

Taxon	Shape factor (K)	Settling speeds (cm/s): Predicted from shape factor	Settling speeds (cm/s): Predicted from mathematical model
Pinus 13:			
With sacci	1.08	2.50	2.60
Without sacci	.97	2.97	2.69
Pinus 25:			
With sacci	1.10	3.22	3.26
Without sacci	1.02	3.73	3.58
Falcatifolium 69:			
With sacci	1.06	2.22	2.23
Without sacci	.98	1.74	1.72
Falcatifolium 83:			
With sacci	1.19	2.27	2.50
Without sacci	.99	2.31	2.21

drag coefficients of textured, main body–only models (i.e., nonsaccate pollen models containing the same type of texture as that on the main body of the saccate models; fig. 7). In these experiments, the drag coefficient curves for the smooth versus textured main body–only models are similar, resulting in no noticeable effect of surface ornamentation. Therefore, the presence of sacci in combination with surface texture lowers the drag coefficient of the pollen models.

To better understand the flow physics that produced the experimental results on surface ornamentation, flow visualization images of the wake behind the pollen models were examined (fig. 8). The smooth sphere showed a single-thread wake, characteristic of laminar, nonseparating flow (fig. 8*a*). A similar wake effect was observed behind the textured main body–only model (i.e., nonsaccate model; fig. 8*b*); recall that the main body was ellipsoidal in geometry (fig. 3). In contrast, the textured saccate model exhibited a dual-thread wake (fig. 8*c*), indicating that the presence of sacci and surface ornamentation have a combined aerodynamic effect. These filaments of dye represent points on the aft of the pollen grain where the flow separates from the model, forming a distinct wake region of stagnant or recirculating flow, depending on Reynolds number. At these low Reynolds numbers, this separation normally would not occur behind spherical geometries. Only at higher Reynolds numbers where inertial effects begin to dominate does flow separation occur, leading to vortex formation.

Variation in relative amount of surface texture. Because no published studies have addressed the effect of surface texture on drag at very low Reynolds numbers, additional experiments were conducted in which texture of varying degrees was applied to simple spheres. This geometry was chosen because data for smooth spheres are the most widely available in the literature. Drag coefficients were measured for smooth spheres, spheres with 4% texture, spheres with 8% texture, and spheres containing conical "spikes" whose length was 12% of the sphere diameter (fig. 9). The textural elements applied to the spheres were also hemispherical, like those applied to the pollen models; however, they were larger in magnitude in order to examine the general effect of texture in low Reynolds number flows. Figure 9 illustrates that for these spherical geometries, surface texture does ultimately result in lower drag coefficients but the effect does not become pronounced unless the texture is fairly significant, as in the case for the spiked sphere.

Discussion

Effects of Pollen Geometry

Dispersion of small, nonspherical particulates of submillimeter scale is relevant to a wide variety of biological, chemical, and industrial applications. Most of the data available on drag coefficients for these particles are experimental and specific to the particular geometry of interest (see Chhabra

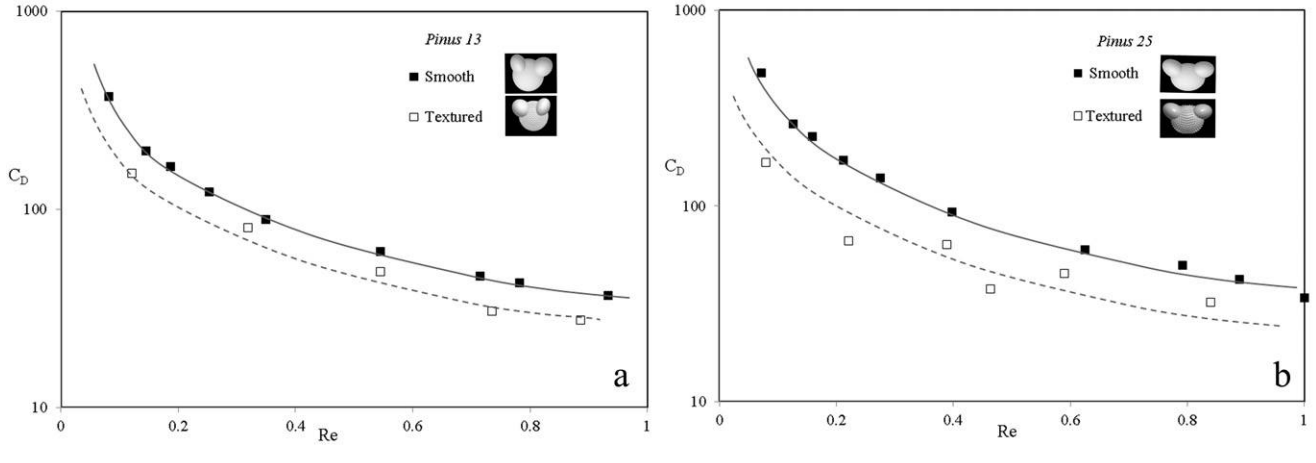

Fig. 6 Effect of surface texture on pollen drag. Drag coefficient (C_D) versus Reynolds number (Re) for *Pinus* models. *a*, *Pinus* 13. *b*, *Pinus* 25. Each pollen type modeled both with smooth main body (filled squares) and with textured main body (open squares). Textured models of grain types exhibited decrease in drag coefficient over a wide range of Reynolds numbers when compared with nontextured, smooth models.

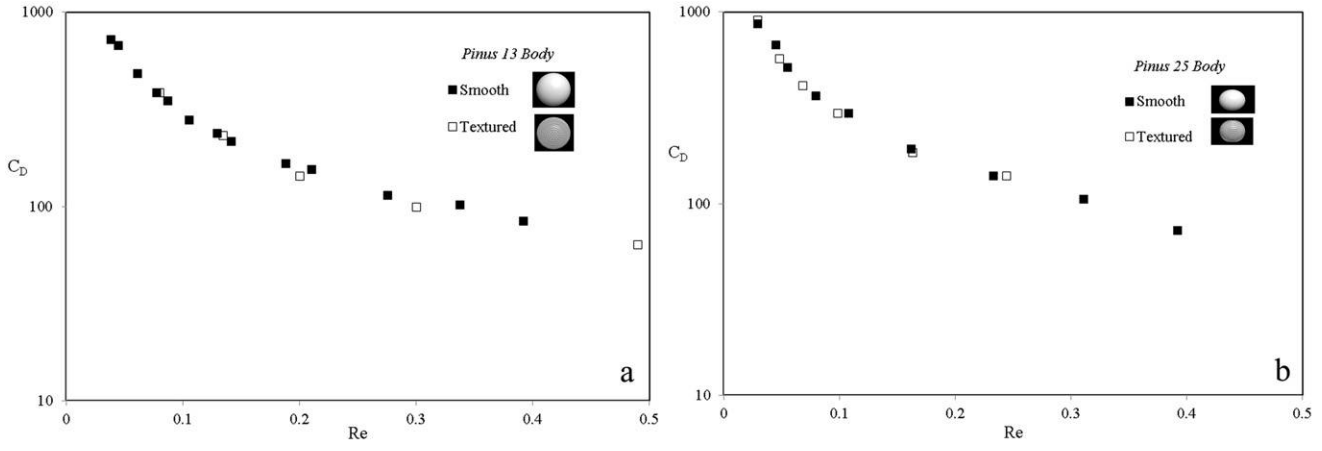

Fig. 7 Effect of surface texture on drag of main body only. Drag coefficient (C_D) versus Reynolds number (Re) for *Pinus* models. *a*, *Pinus* 13. *b*, *Pinus* 25. Drag for smooth versus textured main body–only models was similar, resulting in no noticeable effect of surface ornamentation.

et al. 1999). Several attempts have been made to categorize the available results on the basis of general shape characteristics. Perhaps the most studied nonspherical geometry is the spheroid, which is a sphere elongated in one direction. If the elongation takes place along the flow direction, the spheroid is called prolate; if the elongation is normal (i.e., perpendicular) to the flow direction, the spheroid is oblate. Exact solutions at low Reynolds numbers (below a value of 1), for example, were obtained by Aoi (1955) and Breach (1960), whereas numerical simulations were performed by Masliyah and Epstein (1970), as well as O'Donnell and Helenbrook (2005). Militzer et al. (1989) developed a relatively simple correlation, which related the drag coefficient for spheroidal particles to Reynolds number and aspect ratio (ratio of axial flow dimension divided by the flow-normal dimension). This correlation, which was demonstrated to be accurate over a Reynolds number range of 1–200, represents a convenient means of calculating the drag coefficient (C_D); however, it was not tested for Reynolds numbers below 1.

Regardless of the method used, the general result found for spheroids was that oblate spheroids exhibited drag coefficients that were lower than that of a sphere, whereas the drag coefficients of prolate spheroids were greater than that of a sphere. The reason for this is due to the fact that at very low Reynolds numbers, viscous effects dominate; because the prolate geometry has a longer dimension in the flow direction compared to a sphere, its drag is higher. For the oblate geometry, the corresponding drag is lower because of its flattened dimension in the flow direction.

The pollen grain models in this study, both saccate and nonsaccate (main body only), are, for the most part, ellipsoidal (i.e., all three axis dimensions are different). Principal axis ratios *a*/*b* and *a*/*c* were computed for each pollen model (fig. 3), where *a* represents the maximum length in the flow direction and *b* and *c* represent the maximum model lengths in the plane normal to the flow direction. The models are oblate in one plane and prolate in the other, making it difficult to apply correlations from spheroidal geometries. Drag coefficient data corresponding to a wide range of ellipsoidal geometries are not readily available; however, McNown and Malaika (1950) computed resistance coefficients (a.k.a., shape factors) and presented the results as a family of curves that were a function of the ratio *b*/*c* and a length ratio defined as $a/(bc)^{1/2}$. Shape factors obtained from these curves corresponding to the geometries of the ellipsoidal (i.e., nonsaccate main body–only) models of this study varied between 0.99 and 1.02, which is in excellent agreement with the values obtained from the current experiments (table 2), thus providing validation of the experimental results.

McNown and Malaika (1950) found variations in shape factors from 0.955 (shape of minimal resistance) to greater than 2 for highly elongated ellipsoids. Resistance coefficients were also experimentally determined for prismatic, cylindrical, conical, and ellipsoidal particles by measuring settling velocities. It was found that different shapes of the same proportions (axis ratios) and orientation exhibited similar shape factor (*K*) values, demonstrating that simplified drag corrections could be made for some classes of symmetrical particle shapes. However, only three axis ratios were examined by McNown and Malaika (1950). Wilson and Huang (1979) measured settling velocities of volcanic ash particles and also used simplified shape parameters to collapse drag coefficient data into families of curves.

On the basis of this study's results (fig. 5), the presence of sacci produces a measurable difference in the shape factor, thus demonstrating that sacci clearly play an aerodynamic role in pollen flight at the very low Reynolds numbers associated with these particles. Using these parameters, settling velocities were able to be predicted and compared to those predicted using the mathematical model described in Schwendemann et al. (2007). The excellent agreement between the two methods (table 2) provides an additional measure of empirical validation for the aerodynamic role of sacci. Sacci reduce settling velocities in pollen grains that have primarily air-filled sacci, as in *Pinus*, whereas the presence of sacci may increase settling velocities in pollen grains containing heavier and more dense sacci, due to thick pollen walls and/or extensive endoreticulations, as in *Falcatifolium* (table 2). Regardless of the internal composition of the sacci, their presence increases the pollen grain's flow resistance based on the measured increases

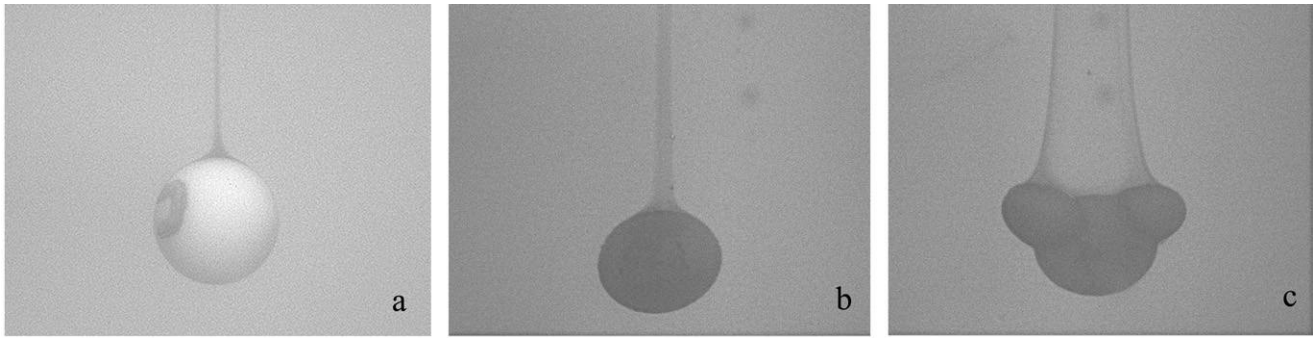

Fig. 8 Flow visualization of wake flow behind pollen models. *a*, Smooth sphere (control) showing single-thread wake, characteristic of laminar, nonseparating flow. *b*, Textured main body only of *Pinus* 25 also showing single-thread wake. *c*, Textured saccate pollen of *Pinus* 25 showing dual-thread wake, indicating that the presence of sacci and surface ornamentation have a combined aerodynamic effect.

in shape factor. Air-filled sacci enhance this effect, resulting in a decrease in settling speed, whereas dense sacci overpower this effect, resulting in an increase in settling speed.

A unique aspect of pollen grains, when compared to other nonspherical solid particulates, is that pollen shape can change while airborne depending on the pollen grain's hydration state (Blackmore and Barnes 1986; Crane 1986). In particular, the angle of orientation of sacci changes as they move closer together to cover the distal aperture to protect the main body against dehydration. Given the variation in measured drag coefficient among the two genera and the four pollen types, it is clear that the aerodynamic characteristics of saccate grains can vary with hydration state, as the angle of orientation of sacci changes. In particular, the two *Pinus* geometries studied exhibited different degrees of sacci orientation. The angles between the major axes of the sacci in *Pinus* 13 and *Pinus* 25 were 80° and 130°, respectively. *Pinus* 13 also exhibited a lower drag coefficient (fig. 4) and lower shape factor (table 2). Additionally, saccus size can vary considerably, both among and within species, as demonstrated by the pollen grains tested in this study. Even though *Falcatifolium* 69 had the largest sacci, these were the most integrated into the main body, whereas *Pinus* 25 and *Falcatifolium* 83 had more structurally distinct sacci, which elongated the pollen grains to a greater degree. For example, in *Falcatifolium* 83, the sacci contributed to the most grain elongation ($a/b = 0.53$; fig. 3). This particular geometry had the largest shape factor, as well as the largest drag coefficient (fig. 4).

One final phenomenon that can occur when irregularly shaped particles fall is that of tumbling. This effect is most pronounced at high Reynolds numbers (i.e., larger, heavier particles), such as the volcanic ash particles studied by Wilson and Huang (1979) in which settling speeds as high as 200 cm/s were measured. In our experiments, no reorientation of the models was observed after they were released in the fluid. McNown and Malaika (1950) examined stability effects of the models, and they found that for very low Reynolds numbers, less than ~0.1, any orientation was stable. At Reynolds numbers higher than this value, particles dropped in a particular orientation tended to orient themselves in a single, stable position. The pollen models and control spheres experimentally examined in this study exhibited Reynolds numbers as high as ~5, and no tumbling motions were detected. Thus, tumbling would not be expected of actual pollen grains in a quiescent fluid (i.e., nonturbulent air).

Effects of Surface Ornamentation

Although surface ornamentation can be very pronounced on some pollen types, this parameter was not included in the original mathematical model by Schwendemann et al. (2007), because drag coefficients at low Reynolds numbers are available only for smooth geometries. Reynolds numbers of the pollen grains measured in Schwendemann et al. (2007) were on the order of 0.01–0.1. At these low Reynolds numbers, the effects of surface roughness are typically neglected in the literature, and such effects on flow characteristics over objects at Reynolds numbers in this low range have not been published. However, Clift et al. (1978) did briefly discuss the effects of surface roughness on drag. The drag-reducing

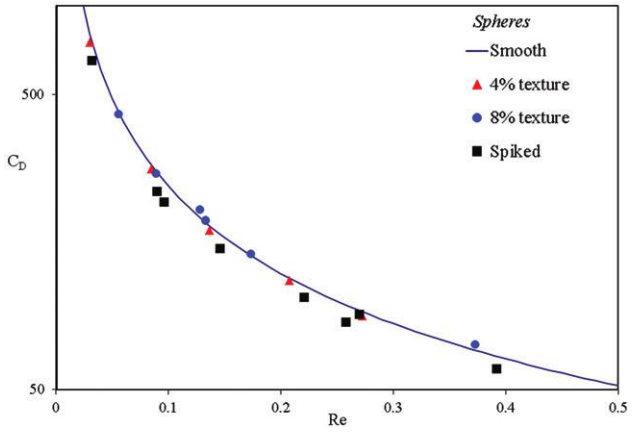

Fig. 9 Effect of surface texture on drag of spheres. Drag coefficient (C_D) versus Reynolds number (Re) for four spheres. Types included smooth spheres, spheres with 4% texture (triangles), spheres with 8% texture (circles), and spheres containing conical "spikes" whose length was 12% of sphere diameter (squares). Surface texture does ultimately result in lower drag coefficients, but the effect does not become pronounced unless the texture is significant, as in spiked sphere.

effects of roughness on spherical objects are most dramatic (and hence most studied) at Reynolds numbers in the critical range, above 50,000, as demonstrated by dimples on a golf ball. At Reynolds numbers on the order of 1000, surface roughness can increase the drag coefficient (C_D), whereas for Reynolds numbers less than 500, large-scale roughness reduces the drag. Clift et al. (1978) suggested that this result should extend into the creeping flow range on the basis of the results of Hill and Power (1956), who showed that the Stokes drag on an arbitrary particle is less than or equal to that on a body that encloses it. This lack of empirical evidence, either supporting or refuting the conjectured reduction of drag on particles at very low Reynolds numbers, represents a void in the existing body of knowledge about drag when applied to any biological entity containing surface texture or other irregularities.

In this study, when texture was applied to the control sphere, it was found that only when the surface ornamentation height exceeded 10% of the sphere's diameter, as in the spiked sphere, did a measurable reduction in drag coefficient occur (fig. 9). In this case, where the Reynolds number range is less than 0.1, the drag coefficient of this sphere with the greatest amount of surface texture was only ~15% lower than that of the smooth sphere (fig. 9). In stark contrast, the differences between the textured and smooth pollen models of *Pinus* were considerably greater (fig. 6), with the effect of texture on the *Pinus* 25 model resulting in a reduction in drag coefficient of ~40%. These data represent the first experimental results published that demonstrate the effect of surface roughness on drag at low Reynolds numbers.

Because the most dramatic reduction in drag was demonstrated on the textured *Pinus* models containing sacci, it was clear that the presence of sacci contributed to this increased reduction, likely by altering flow patterns near the surface of the main body. While a more detailed explanation into the flow physics producing the results generated from these experiments would require computational simulations or measurements of the flow field around a pollen model containing the appropriate surface ornamentation, key fundamental insight was gained in this study from flow visualization of the wake behind the models. The flow data demonstrated an increased separation region in the wake of the saccate pollen model when compared to both an ellipsoid (the nonsaccate, main body–only model) and a sphere (control; fig. 8). Prior to the flow separating around the saccate pollen model, the flow pattern would be continuously decelerating close to the surface, thereby reducing viscous stresses around the main body and hence contributing to lower drag.

When considered in combination with pollen geometry, the effects of surface ornamentation and the presence of sacci on aerodynamic properties are more pronounced. In this study, the settling speeds of the pollen grains predicted using the experimental shape factors were found to be in excellent agreement with those obtained from the mathematical model (table 2). In both of these cases, texture was not incorporated into the analysis. On the basis of the lower drag coefficients obtained on the textured pollen models (fig. 6), texture would further increase settling speeds above the predicted values. The unique shape of the pollen models, due to the presence of sacci, contributed to this increase in settling speeds, as the effect of texture on the spheres studied did not produce as dramatic a reduction in drag coefficient, even with significantly higher levels of texture (fig. 9).

Therefore, on the basis of the experimental results of this study, it is clear that both sacci and surface ornamentation are necessary characters that must be incorporated into accurate predictions of pollen aerodynamics. Given the novelty of these results on the effect of surface ornamentation at low Reynolds numbers, additional studies are warranted in order to expand on this flow regime.

Conclusions

An experimental investigation was conducted that examined the effects of both geometry and surface ornamentation on pollen drag and settling velocities. Sacci increased the shape factor, or resistance coefficient, in all of the pollen types studied, compared to the same pollen types that had been modeled without sacci. Two characters contributed to this: the orientation of the sacci, or angle between the sacci's major axes, and the size of the sacci relative to the main body. On the basis of the shape factors obtained from smooth pollen models, the experimental data provided additional validation of the mathematical model developed previously by Schwendemann et al. (2007). In particular, the presence of sacci decreased settling velocities in *Pinus*, whose sacci add minimal mass and appreciable volume to the grain, whereas sacci increased settling velocities in *Falcatifolium*, whose sacci add significant mass and volume to the grain.

Novel to this study was the ability to incorporate surface texture onto the pollen models in order to isolate the aerodynamic effect of this character. The presence of surface ornamentation on the main body decreased the drag coefficients on the saccate pollen grains of *Pinus*; this effect was clearly evident when compared to pollen grains that were modeled with a smooth surface. This study is the first to experimentally demonstrate the effect of surface texture on drag for biological or nonbiological particles at low Reynolds numbers. Results from this study demonstrate that accurate modeling of pollen settling velocities requires the incorporation of both geometrical and textural attributes.

This study provides additional empirical evidence for the aerodynamic role of sacci, supporting their adaptive significance for wind pollination. This study demonstrates that sacci, along with surface ornamentation, clearly play a role in anemophily in some saccate taxa. In addition to the aerodynamic role, it is also clear that sacci may have a flotation role and that this function has been the subject of selective pressure in some saccate taxa. The suite of empirical studies that is now available supporting both the aerodynamic and buoyancy functions of sacci provides the opportunity to probe a range of evolutionary questions about extant and extinct seed plants that have been unavailable heretofore.

Acknowledgments

We are grateful to Thomas N. Taylor (University of Kansas) for his significant and extensive research, his pioneering research in paleopalynology, his influential and leadership role in paleobotany, and his enduring friendship. He

continues to be an inspiration to us. We also thank Andrew Caden, Christopher Durando, Dennis O'Connell, Thomas Samper, and Bhumi Shah (all from the College of New Jersey) for their contributions to the research. This study was supported in part by the College of New Jersey and the National Science Foundation.

Literature Cited

Aoi T 1955 The steady flow of viscous fluid past a fixed spheroidal obstacle at small Reynolds numbers. J Phys Soc Jpn 10: 119–129.

Blackmore S, SH Barnes 1986 Harmomegathic mechanisms in pollen grains. Pages 137–149 *in* S Blackmore, IK Ferguson, eds. Pollen and spores: form and function. Academic Press, London.

Breach DR 1960 Slow flow past ellipsoids of revolution. J Fluid Mech 10:306–314.

Chhabra RP, L Agarwal, NK Sinha 1999 Drag on nonspherical particles: an evaluation of available methods. Powder Technol 101: 288–295.

Chung JN, TR Trout 1988 Simulation of particle dispersion in an axisymmetric jet. J Fluid Mech 186:199–222.

Clift R, JR Grace, ME Weber 1978 Bubbles, drops, and particles. Academic Press, New York.

Crane PR 1986 Form and function in wind dispersed pollen. Pages 179–202 *in* S Blackmore, IK Ferguson, eds. Pollen and spores: form and function. Academic Press, London.

Happel J, E Bart 1974 Settling of a sphere along the axis of a long square duct at low Reynolds number. Appl Sci Res 29:241–258.

Hill R, G Power 1956 Extremeum principles for slow viscous flow and the approximate calculation of drag. Q J Mech Appl Math 9: 313–319.

Leslie AB 2010 Flotation preferentially selects saccate pollen during conifer pollination. New Phytol 188:273–279.

Loth E 2008 Drag of nonspherical particles of regular and irregular shape. Powder Technol 182:342–353.

Masliyah JH, N Epstein 1970 Numerical study of steady flow past spheroids. J Fluid Mech 44:493–512.

McNown JS, J Malaika 1950 Effects of particle shape on settling velocity at low Reynolds numbers. EOS Trans Am Geophys Union 31:74–82.

Militzer J, JM Kan, F Hamdullahpur, PR Amyotte, AM Al Taweel 1989 Drag coefficients for axisymmetric flow around individual spheroidal particles. Powder Technol 57:193–195.

Murphy D, V Cherkaduvasala, K Harrison, L Monroe, H Ban 2002 Evaluation of drag coefficients of coal ash particles. Proc ASME Fluids Eng Div 258:645–651.

Niklas KJ 1984 The motion of windborne pollen grains around ovulate cones: implication on wind pollination. Am J Bot 71: 356–374.

——— 1985*a* The aerodynamics of wind pollination. Bot Rev 51: 328–386.

——— 1985*b* Wind pollination: a study in controlled chaos. Am Sci 73:462–470.

Niklas KK, KT Paw U 1982 Pollination and airflow patterns around conifer ovulate cones. Science 217:442–444.

O'Donnell BJ, BT Helenbrook 2005 Drag on ellipsoids at finite Reynolds numbers. At Sprays 15:363–375.

Osborn JM, TN Taylor 1994 Comparative ultrastructure of fossil gymnosperm pollen and its phylogenetic implications. Pages 99–121 *in* MH Kurmann, JA Doyle, eds. Ultrastructure of fossil spores and pollen. Royal Botanic Gardens, Kew.

Proctor M, P Yeo, A Lack 1996 The natural history of pollination. Timber, Portland, OR.

Runions CJ, KH Rensing, T Takaso, JN Owen 1999 Pollination of *Picea orientalis* (Pinaceae): saccus morphology governs pollen buoyancy. Am J Bot 86:190–197.

Schwendemann AB, G Wang, ML Mertz, RT McWilliams, SL Thatcher, JM Osborn 2007 Aerodynamics of saccate pollen and its implications for wind pollination. Am J Bot 94:1371–1381.

Stokes GG 1851 On the effect of the inertial friction of fluids on the motion of pendulums. Trans Cambr Philos Soc 9:8–106.

Taylor TN, EL Taylor, M Krings 2009 Paleobotany: the biology and evolution of fossil plants. 2nd ed. Academic Press, Amsterdam.

Tomlinson PB 1994 Functional morphology of saccate pollen in conifers with special reference to Podocarpaceae. Int J Plant Sci 155: 699–715.

——— 2000 Structural features of saccate pollen types in relation to their function. Pages 147–162 *in* MM Harley, CM Morton, S Blackmore, eds. Pollen and spores: morphology and biology. Royal Botanical Gardens, Kew.

Vogel S 1994 Life in moving fluids: the physical biology of flow. 2nd ed. Princeton University Press, Princeton, NJ.

Whitehead DR 1983 Wind pollination: some ecological and evolutionary perspectives. Pages 97–108 *in* L Real, ed. Pollination biology. Academic Press, Orlando, FL.

Wilson L, TC Huang 1979 The influence of shape on the atmospheric settling velocity of volcanic ash particles. Earth Planet Sci Lett 44:311–324.

Wodehouse RP 1935 Pollen grains: their structure, identification and significance in science and medicine. Hafner, New York.